International Journal of Heat and Mass Transfer 53 (2010) 4316–4325

Contents lists available at ScienceDirect

International Journal of Heat and Mass Transfer

journal homepage: www.elsevier.com/locate/ijhmt

Analysis of temperature gradient bifurcation in porous media – An exact solution

Kun Yang [a,b], Kambiz Vafai [b,*]

[a] School of Energy and Power Engineering, Huazhong University of Science and Technology, Wuhan 430074, PR China
[b] Department of Mechanical Engineering, University of California Riverside, Riverside, CA 92521-0425, USA

ARTICLE INFO

Article history:
Received 24 March 2010
Received in revised form 1 May 2010
Accepted 1 May 2010
Available online 16 June 2010

Keywords:
Porous media
Convective heat transfer
Internal heat generation
Local thermal non-equilibrium

ABSTRACT

The phenomenon of temperature gradient bifurcation in a porous medium is analyzed by studying the convective heat transfer process within a channel filled with a porous medium, with internal heat generation. A local thermal non-equilibrium (LTNE) model is used to represent the energy transport within the porous medium. Exact solutions are derived for both the fluid and solid temperature distributions for two primary approaches (Models A and B) for the constant wall heat flux boundary condition. The Nusselt number for the fluid at the channel wall is also obtained. The effects of the pertinent parameters such as fluid and solid internal heat generations, Biot number and fluid to solid thermal conductivity ratio are discussed. It is shown that the internal heat generation in the solid phase is significant for the heat transfer characteristics. The validity of the one equation model is investigated by comparing the Nusselt number obtained from the LTNE model with that from the local thermal equilibrium (LTE) model. The results demonstrate the importance of utilizing the LTNE model in the present study. The phenomenon of temperature gradient bifurcation for the fluid and solid phases at the wall for Model A is established and demonstrated. In addition, the temperature distributions for Models A and B are compared. A numerical study for the constant temperature boundary condition was also carried out. It was established that the phenomenon of temperature gradient bifurcation for the fluid and solid phases for the constant temperature boundary condition can occur over a given axial region.

1. Introduction

Convective heat transfer in porous media is encountered in a wide variety of industrial applications such as thermal energy storage, nuclear waste repository, electronic cooling, geothermal energy utilization, petroleum industry and heat transfer enhancement. A number of situations involve internal heat generation such as nuclear reactor applications, agricultural product storage, electronic cooling, or a solar air heater packed with a porous medium where the packed material provides the heat transfer enhancement and also acts as an absorbing media for the solar radiation [1].

Two primary models can be utilized for representing heat transfer in a porous medium: LTE and LTNE, which incorporates the temperature difference between the fluid and solid phases, thus resulting in different energy equations for the fluid and solid phases. Amiri and Vafai [2] employed a generalized model for the momentum equation and LTNE to investigate the forced convective heat transfer within a channel with a constant wall temperature. They investigated in detail the inertial and boundary effects, porosity variation, thermal dispersion and the validity of local thermal equilibrium as well as other pertinent effects. Amiri et al. [3] presented for the first time two primary approaches for the constant wall heat flux boundary conditions under the local thermal non-equilibrium condition in porous media. Based on the two-equation model (LTNE), and using one of the two primary approaches given in Amiri et al. [3], Lee and Vafai [4] investigated the forced convective flow through a channel filled with a porous medium subject to a constant heat flux, and derived exact solutions for both fluid and solid phase temperature fields. Marafie and Vafai [5] obtained analytical solutions for the fluid and solid phase temperature distributions for the forced convective flow through a channel filled with a porous medium with a constant heat flux boundary condition, in which the Brinkman–Forchhiemer-extended Darcy equation was used to obtain the velocity field. Alazmi and Vafai [6] presented a comprehensive analysis of the effect of using different boundary conditions for the case of constant wall heat flux under the local thermal non-equilibrium condition.

The main objective of the present study is to analyze the temperature gradient bifurcation phenomenon in porous media by investigating the heat transfer characteristics for convection through a channel filled with a porous medium, with internal heat generation in both the fluid and solid phases, and subject to a constant heat flux boundary condition. The analytical solutions for the fluid and solid phase temperature distributions and the Nusselt number at the channel wall are obtained. The effects of pertinent

* Corresponding author.
E-mail address: vafai@engr.ucr.edu (K. Vafai).

0017-9310/$ - see front matter © 2010 Elsevier Ltd. All rights reserved.
doi:10.1016/j.ijheatmasstransfer.2010.05.060

Nomenclature

Bi	$Bi = \frac{h_i \alpha H^2}{k_{s,eff}}$, Biot number defined by Eq. (13)
c_p	specific heat of the fluid [J kg^{-1} K^{-1}]
E	$E = \frac{Nu_1 - Nu}{Nu}$, error in the Nusselt number defined by Eq. (73)
h_i	interstitial heat transfer coefficient [W m^{-2} K^{-1}]
h_w	wall heat transfer coefficient defined by Eq. (25) [W m^{-2} K^{-1}]
h_{w1}	wall heat transfer coefficient calculated from one equation model, defined by Eq. (32) [W m^{-2} K^{-1}]
H	half height of the channel [m]
k	$k = \frac{k_{f,eff}}{k_{s,eff}}$, ratio of the fluid effective thermal conductivity to that of the solid, defined by Eq. (12)
$k_{f,eff}$	effective thermal conductivity of the fluid [W m^{-1} K^{-1}]
$k_{s,eff}$	effective thermal conductivity of the solid [W m^{-1} K^{-1}]
Nu	Nusselt number for the LTNE model, defined by Eq. (26)
Nu_1	Nusselt number for the LTE model, defined by Eq. (33)
q_w	heat flux at the wall [W m^{-2}]
Q	integrated internal heat transfer exchange between the solid and fluid phases [W m^{-2}]
Re	$Re = \frac{u(4H)}{\nu_f}$, Reynolds number
S_f	internal heat generation within the fluid phase [W m^{-3}]
S_s	internal heat generation within the solid phase [W m^{-3}]
T	temperature [K]
u	fluid velocity [m s^{-1}]
x	longitudinal coordinate [m]
y	transverse coordinate [m]

Greek symbols

$\Delta\theta$	non-dimensional temperature difference, $\Delta\theta = \theta_s - \theta_f$
α	interfacial area per unit volume of the porous medium [m^{-1}]
β	$\beta = \frac{S_s H}{q_w}$, parameter defined by Eq. (14)
β_1	$\beta_1 = \frac{\lambda}{(1+k)\tanh(\lambda)} - \frac{1}{1+k}$, parameter defined by Eq. (56)
β_2	$\beta_2 = -\frac{\lambda k}{(1+k)\tanh(\lambda)} - \frac{1}{1+k}$, parameter defined by Eq. (57)
β_3	$\beta_3 = -\frac{Bi}{3\left[1 - \frac{1}{\lambda}\tanh(\lambda)\right]} - \frac{1}{1+k}$, parameter defined by Eq. (70)
η	non-dimensional transverse coordinate, defined by Eq. (6b)
ξ	non-dimensional axial length scale, defined by Eq. (51)
θ	non-dimensional temperature, defined by Eq. (6a) for Model A, defined by Eqs. (36) and (37) for Model B, or defined by Eq. (50) for constant temperature case
θ_b	non-dimensional bulk mean temperature for the LTE model
$\theta_{f,b}$	non-dimensional bulk mean temperature of the fluid, defined by Eq. (24)
λ	parameter defined by Eq. (21)
ρ	fluid density [kg m^{-3}]

Subscripts

f	fluid phase
s	solid phase
w	wall

Other symbols

$\langle\rangle$	average over the channel cross section

parameters such as internal heat generation, Biot number and thermal conductivity ratio are discussed. By comparing the Nusselt number obtained from the two-equation (LTNE) model with that from the one equation (LTE) model, the validity of the one equation model is investigated. In addition, the temperature distributions for two different approaches (Models A and B) for the constant wall heat flux boundary condition are compared. Furthermore, a numerical study for the constant temperature boundary condition was also carried out to investigate the temperature gradient bifurcation for that case. To the best of authors' knowledge, the present analysis of the temperature gradient bifurcation in porous medium is presented for the first time in the literature.

2. Modeling and formulation

The schematic diagram of the problem is shown in Fig. 1. Fluid flows through a rectangular channel filled with a porous medium subject to a constant heat flux boundary condition. We consider uniform but different internal heat generations in both the solid and fluid phases, S_s and S_f, respectively. The height of the channel is $2H$ and the heat flux applied at the wall is q_w. The following assumptions are invoked in analyzing this problem.

(1) The flow is steady and incompressible.
(2) Natural convection and radiative heat transfer are negligible.
(3) Properties such as porosity, specific heat, density and thermal conductivity are assumed to be constant.
(4) Thermally developed condition is considered and the fluid flow is represented by the Darcian flow model.

Based on these assumptions, the following governing equations are obtained from the works of Amiri et al. [2,3] employing the local thermal non-equilibrium model.

Fluid phase

$$k_{f,eff}\frac{\partial^2 T_f}{\partial y^2} + h_i\alpha(T_s - T_f) + S_f = \rho c_p u\frac{\partial T_f}{\partial x} \tag{1}$$

Solid phase

$$k_{s,eff}\frac{\partial^2 T_s}{\partial y^2} - h_i\alpha(T_s - T_f) + S_s = 0 \tag{2}$$

where T_f and T_s are the fluid and solid temperatures, u the fluid velocity, $k_{f,eff}$ and $k_{s,eff}$ the effective fluid and solid thermal conductivities, respectively, ρ and c_p the density and specific heat of the fluid, h_i the interstitial heat transfer coefficient, and α is the interfacial area per unit volume of the porous medium.

2.1. Boundary conditions [Model A]

When a solid substrate of finite thickness and high thermal conductivity is attached to the porous medium as shown in Fig. 1., the

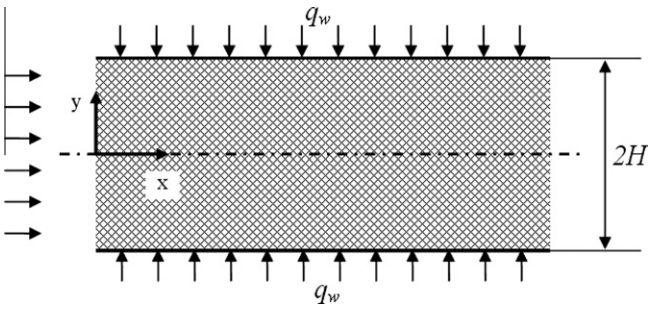

Fig. 1. Schematic diagram for flow through a channel filled with a porous medium and the corresponding coordinate system.

temperature of the solid and the fluid at the wall interface will be the same [4,5].

$$T_f|_{y=H} = T_s|_{y=H} = T_w \tag{3}$$

where T_w is the temperature at the wall interface. Based on the work of Amiri et al. [3], the total heat flux q_w will be divided between the fluid and solid phases depending on the physical values of their effective conductivities and their corresponding temperature gradients at the wall.

$$q_w = k_{f,eff}\left.\frac{\partial T_f}{\partial y}\right|_{y=H} + k_{s,eff}\left.\frac{\partial T_s}{\partial y}\right|_{y=H} \tag{4}$$

In this part, we utilize the approach for the constant heat flux boundary condition given by Eqs. (3) and (4) and discussed in detail in Amiri et al. [3] and Alazmi and Vafai [6] as Model A. Due to the symmetry condition at the center of the channel, the following boundary condition can be used:

$$\left.\frac{\partial T_f}{\partial y}\right|_{y=0} = \left.\frac{\partial T_s}{\partial y}\right|_{y=0} = 0 \tag{5}$$

2.2. Normalization

To normalize the governing equation and the boundary conditions, the following dimensionless variables are introduced:

$$\theta = \frac{k_{s,eff}(T - T_w)/H}{q_w} \tag{6a}$$

$$\eta = \frac{y}{H} \tag{6b}$$

Adding governing Eqs. (1) and (2), and integrating the resultant equation from the center to the wall and applying the boundary conditions given by Eqs. (3)–(5), the following equation is obtained.

$$\rho c_p \langle u \rangle \left\langle \frac{\partial T_f}{\partial x} \right\rangle = \frac{q_w}{H} + S_f + S_s \tag{7}$$

where $\langle\rangle$ refers to the area average over the channel cross section. Using Eqs. (6) and (7), and the Darcian flow model, the governing Eqs. (1) and (2) and boundary conditions (3) and (5) can be rewritten as:

$$k\frac{\partial^2 \theta_f}{\partial \eta^2} + Bi(\theta_s - \theta_f) = 1 + \beta \tag{8}$$

$$\frac{\partial^2 \theta_s}{\partial \eta^2} - Bi(\theta_s - \theta_f) + \beta = 0 \tag{9}$$

$$\theta_f|_{\eta=1} = \theta_s|_{\eta=1} = 0 \tag{10}$$

$$\left.\frac{\partial \theta_f}{\partial \eta}\right|_{\eta=0} = \left.\frac{\partial \theta_s}{\partial \eta}\right|_{\eta=0} = 0 \tag{11}$$

where the thermal conductivity ratio, k, Biot number, Bi and β are defined as:

$$k = \frac{k_{f,eff}}{k_{s,eff}} \tag{12}$$

$$Bi = \frac{h_i \alpha H^2}{k_{s,eff}} \tag{13}$$

$$\beta = \frac{S_s H}{q_w} \tag{14}$$

Based on Eqs. (8)–(14), it is obvious that the uniform internal heat generation in the fluid phase, S_f, has no influence on the dimensionless temperature distributions, θ_s and θ_f. However, S_f has an influence on the dimensional temperature distributions, T_s and T_f.

2.3. Temperature distribution

Utilizing the two coupled governing Eqs. (8) and (9), which involve two unknown functions, θ_f andθ_s, the following governing equations for the fluid and solid temperatures are obtained.

$$k\theta_f'''' - (1+k)Bi\theta_f'' = -Bi \tag{15}$$

$$k\theta_s'''' - (1+k)Bi\theta_s'' = -Bi \tag{16}$$

Two more sets of boundary conditions are required to solve the above fourth-order differential equations in addition to the boundary conditions given by Eqs. (10) and (11). By utilizing the boundary conditions (10) and (11) in Eqs. (8) and (9), the following equations are obtained.

$$\theta_f''(1) = (1+\beta)/k, \quad \theta_s''(1) = -\beta \tag{17}$$

$$\theta_f'''(0) = \theta_s'''(0) = 0 \tag{18}$$

The temperature distribution is found by solving Eqs. (15) and (16) and applying the boundary Eqs. (10), (11), (17) and (18). The resultant equations are

$$\theta_f = \frac{1}{1+k}\left\{\frac{1}{2}(\eta^2 - 1) + \left(\frac{1}{1+k} + \beta\right)\frac{1}{Bi}\left[\frac{\cosh(\lambda\eta)}{\cosh(\lambda)} - 1\right]\right\} \tag{19}$$

$$\theta_s = \frac{1}{1+k}\left\{\frac{1}{2}(\eta^2 - 1) + \left(\frac{1}{1+k} + \beta\right)\frac{k}{Bi}\left[1 - \frac{\cosh(\lambda\eta)}{\cosh(\lambda)}\right]\right\} \tag{20}$$

$$\text{where, } \lambda = \sqrt{Bi(1+k)/k} \tag{21}$$

When there is no internal heat generation in a porous medium, $\beta = 0$, and Eqs. (19) and (20) will transform into the analytical expressions given in Lee and Vafai [4]. Based on Eqs. (19) and (20), the temperature difference between the solid and fluid phases is derived as:

$$\Delta\theta|_{Model\,A} = \theta_s - \theta_f = \left(\frac{1}{1+k} + \beta\right)\frac{1}{Bi}\left[1 - \frac{\cosh(\lambda\eta)}{\cosh(\lambda)}\right] \tag{22}$$

Considering when $\frac{\partial|\Delta\theta|}{\partial\eta} = 0$, the maximum $|\Delta\theta|$ is derived as:

$$|\Delta\theta|_{Model\,A,\max} = \left|\frac{1}{1+k} + \beta\right|\frac{1}{Bi}\left[1 - \frac{1}{\cosh(\lambda)}\right] \tag{23}$$

2.4. Nusselt number expressions

Using Eq. (19), the non-dimensional bulk mean temperature of the fluid can be calculated as

$$\theta_{f,b} = \frac{\int_0^1 \theta_f(\eta) u d\eta}{\langle u \rangle} = -\frac{1}{1+k}\left\{\frac{1}{3} + \left(\frac{1}{1+k} + \beta\right)\frac{1}{Bi}\left[1 - \frac{1}{\lambda}\tanh(\lambda)\right]\right\} \tag{24}$$

The wall heat transfer coefficient is obtained from

$$h_w = \frac{q_w}{T_w - T_{f,b}} \tag{25}$$

and the Nusselt number from

$$Nu = \frac{h_w(4H)}{k_{f,eff}} = -\frac{4}{k\theta_{f,b}} \tag{26}$$

where 4H is the hydraulic diameter of the channel. Substituting Eq. (24) in Eq. (26), results

$$Nu = \frac{4(1+k)}{k}\left\{\frac{1}{3} + \left(\frac{1}{1+k} + \beta\right)\frac{1}{Bi}\left[1 - \frac{1}{\lambda}\tanh(\lambda)\right]\right\}^{-1} \tag{27}$$

2.5. One equation model

The governing equation for the one equation model can be obtained by adding Eqs. (8) and (9), and assuming that the temperatures of the fluid and solid phases are the same. This result in

$$(k+1)\frac{\partial^2\theta}{\partial\eta^2}=1 \tag{28}$$

The corresponding boundary conditions are

$$\theta|_{\eta=1}=0 \tag{29}$$

$$\left.\frac{\partial\theta}{\partial\eta}\right|_{\eta=0}=0 \tag{30}$$

The temperature distribution for the one equation model is derived as

$$\theta=\frac{1}{2(1+k)}(\eta^2-1) \tag{31}$$

The wall heat transfer coefficient for the one equation model is obtained from

$$h_{w1}=\frac{q_w}{T_w-T_b} \tag{32}$$

where T_b is bulk mean temperature of the fluid. The Nusselt number for the one equation model is obtained as

$$Nu_1=\frac{h_{w1}(4H)}{k_{f,eff}}=-\frac{4}{k\theta_b}=12\frac{1+k}{k} \tag{33}$$

Unlike the LTNE model, Eqs. (31) and (33) show that the uniform internal heat generation in porous media has no influence on the dimensionless temperature distribution, θ, and the Nusselt number, Nu_1, for the LTE model. However, the heat generation plays a role in the dimensional temperature distribution for the LTE model.

2.6. Analytical solutions for the other primary constant heat flux boundary condition [Model B]

The other primary approach for handling the constant wall heat flux boundary is also based on the work presented by Amiri et al. [3] and analyzed in detail in Alazmi and Vafai [6]. For this case, [Model B], the fluid phase or the solid phase at the wall are each exposed to a heat flux q_w. The corresponding representation for Model B is given by

$$q_{s,w}=k_{s,eff}\left.\frac{\partial T_s}{\partial y}\right|_{y=H}=q_w \tag{34}$$

$$q_{f,w}=k_{f,eff}\left.\frac{\partial T_f}{\partial y}\right|_{y=H}=q_w \tag{35}$$

The above approach for incorporating a constant heat flux boundary condition represented by Eqs. (34) and (35), is defined as Model B.

It should be noticed that the temperature of the solid and the fluid at the wall interface may not be the same based on the boundary conditions (34) and (35). Therefore, the dimensionless temperature for the solid and fluid phases are redefined as

$$\theta_s=\frac{k_{s,eff}(T_s-T_{s,w})/H}{q_w} \tag{36}$$

$$\theta_f=\frac{k_{s,eff}(T_f-T_{s,w})/H}{q_w} \tag{37}$$

where $T_{s,w}$ is the solid temperature at the wall. Adding governing Eqs. (1) and (2), and integrating the resultant equation from the center to the wall and applying the boundary conditions given by Eqs. (5), (34) and (35), the following equation is obtained.

$$\rho c_p\langle u\rangle\left\langle\frac{\partial T_f}{\partial x}\right\rangle=\frac{2q_w}{H}+S_f+S_s \tag{38}$$

Using Eqs. (6b), (36), (37) and (38), and the Darcian flow model, the governing Eqs. (1) and (2) and boundary conditions (5), (34) and (35) can be rewritten as:

$$k\frac{\partial^2\theta_f}{\partial\eta^2}+Bi(\theta_s-\theta_f)=2+\beta \tag{39}$$

$$\frac{\partial^2\theta_s}{\partial\eta^2}-Bi(\theta_s-\theta_f)+\beta=0 \tag{40}$$

$$\left.\frac{\partial\theta_f}{\partial\eta}\right|_{\eta=0}=\left.\frac{\partial\theta_s}{\partial\eta}\right|_{\eta=0}=0 \tag{41}$$

$$\left.\frac{\partial\theta_f}{\partial\eta}\right|_{\eta=1}=\frac{1}{k} \tag{42}$$

$$\theta_s|_{\eta=1}=0 \tag{43}$$

Based on Eqs. (39)–(43), it can be deduced that the uniform internal heat generation in the fluid phase, S_f, has again no influence on the dimensionless temperature distributions, θ_s and θ_f, when Model B is used in applying the constant heat flux boundary condition. The temperature distribution is found by solving Eqs. (39) and (40) and applying the boundary Eqs. (41)–(43). The resultant equations are

$$\theta_f=\frac{1-k}{(1+k)\lambda\sinh(\lambda)}\left[\frac{\cosh(\lambda\eta)}{k}+\cosh(\lambda)\right]+\frac{\eta^2-1}{1+k}-\frac{2}{(1+k)Bi}-\frac{\beta}{Bi} \tag{44}$$

$$\theta_s=\frac{1-k}{(1+k)\lambda\sinh(\lambda)}[\cosh(\lambda)-\cosh(\lambda\eta)]+\frac{\eta^2-1}{1+k} \tag{45}$$

Based on Eq. (45), it is found that the uniform internal heat generation in the solid phase, S_s, has no influence on the dimensionless solid temperature distribution, θ_s, when Model B is used for the constant heat flux boundary condition. Furthermore, S_f has no influence on either θ_s or θ_f. However, again the heat generations have an influence on the dimensional temperature distributions. The temperature difference between the solid and fluid phases, when Model B is used for the constant heat flux, is derived as:

$$\Delta\theta|_{ModelB}=\theta_s-\theta_f=\frac{k-1}{(1+k)\lambda\sinh(\lambda)}\left[\frac{\cosh(\lambda\eta)}{k}+\cosh(\lambda\eta)\right]+\frac{2}{(1+k)Bi}+\frac{\beta}{Bi} \tag{46}$$

2.7. Constant temperature boundary condition

The temperature gradient bifurcation was also examined numerically for the constant temperature boundary condition, while incorporating the axial conduction. The corresponding boundary conditions for the constant temperature condition were expressed as

$$T_f|_{y=H}=T_s|_{y=H}=T_w \tag{47}$$

$$\left.\frac{\partial T_f}{\partial y}\right|_{y=0}=\left.\frac{\partial T_s}{\partial y}\right|_{y=0}=0 \tag{48}$$

$$T_f|_{x=0}=T_s|_{x=0}=T_{in} \tag{49}$$

The governing equations and the boundary conditions are solved using a finite difference method. Upwind discretization scheme is used for the convection term and central differencing

is used for diffusion terms. Variable and uniform grid distributions were used for the y and x-directions, respectively. The convergence was assumed to have been reached when the relative variation of the temperature between two successive iterations was less than 10^{-10}. The sensitivity to the grid interval and the convergence criteria were examined to insure grid independence results. The following dimensionless variables were introduced to show the results for this case.

$$\theta = \frac{k_{s,eff}(T - T_w)}{S_s H^2} \tag{50}$$

$$\xi = \frac{x}{H} \tag{51}$$

$$Re = \frac{u(4H)}{\nu_f} \tag{52}$$

3. Results and discussion

The dimensionless temperature distributions for the fluid and solid phases for Model A for different pertinent parameters β, Bi and k are shown in the Figs. 2 and 3. When Bi is small, which translates into a weak internal heat transfer between the fluid and solid phases, the temperature difference between the two phases is relatively large, especially for a small k, as shown in Figs. 2(a) and 3(a). As k increases, the influence of the fluid thermal conduction becomes significant over most of the channel.

It is important to note that the direction of the temperature gradient for the fluid and solid phases for Model A are different at the wall ($\eta = 1$) in Fig. 2(c) and (d) and Fig. 3(a) (b) and (c). This leads to a temperature gradient bifurcation for Model A for those cases. From Eqs. (19) and (20), the temperature gradients at the wall for the fluid and solid for Model A are obtained as:

$$\theta_f'(1) = \frac{1}{1+k} + \left[\frac{1}{(1+k)k} + \frac{\beta}{k}\right]\frac{1}{\lambda}\tanh(\lambda) \tag{53}$$

$$\theta_s'(1) = \frac{1}{1+k} - \left[\frac{1}{(1+k)} + \beta\right]\frac{1}{\lambda}\tanh(\lambda) \tag{54}$$

If β satisfies the following condition, the direction of the temperature gradients for Model A at the wall for fluid and solid phases are different.

$$\beta > \beta_1 \quad \text{or} \quad \beta < \beta_2 \tag{55}$$

$$\text{where, } \beta_1 = \frac{\lambda}{(1+k)\tanh(\lambda)} - \frac{1}{1+k} \tag{56}$$

$$\beta_2 = -\frac{\lambda k}{(1+k)\tanh(\lambda)} - \frac{1}{1+k} \tag{57}$$

It should be noted that $\frac{\lambda}{\tanh(\lambda)} > 1$ for $\lambda > 0$. Therefore, $\beta_1 > 0$, and $\beta_2 < -1$. The variations of β_1 and β_2 as a function of pertinent parameters Bi and k for Model A are shown in Figs. 4 and 5. β_1 is found to increase as Bi becomes larger and k becomes smaller, while β_2 decreases as Bi becomes larger.

When Model A is used for the constant wall heat flux boundary condition, the integrated internal heat transfer exchange between the solid and fluid phases is obtained from

$$Q = \int_0^h h_i \alpha (T_s - T_f) dy = q_w \int_0^1 Bi(\theta_s - \theta_f) d\eta \tag{58}$$

Substituting Eq. (22) in Eq. (58), results in

$$Q = q_w \left(\frac{1}{1+k} + \beta\right)\left[1 - \frac{\tanh(\lambda)}{\lambda}\right] \tag{59}$$

The heat flux at the wall for the solid phase is obtained from

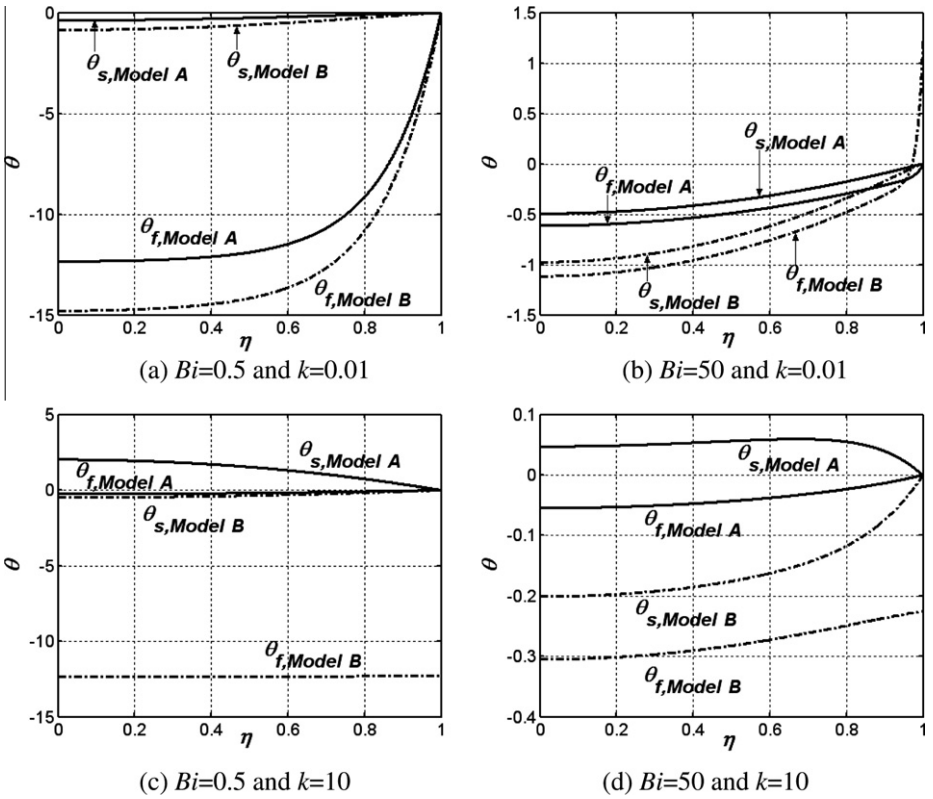

Fig. 2. Dimensionless temperature distributions for fluid and solid phases for Models A and B for: $\beta = 5$ (a) $Bi = 0.5$ and $k = 0.01$; (b) $Bi = 50$ and $k = 0.01$; (c) $Bi = 0.5$ and $k = 10$; (d) $Bi = 50$ and $k = 10$.

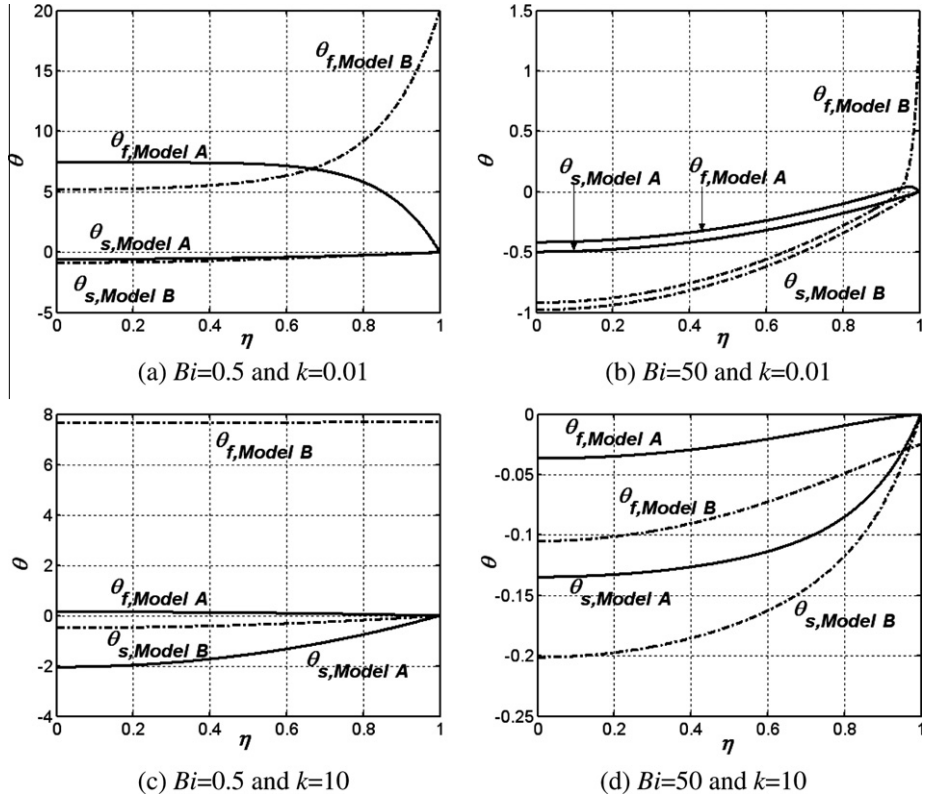

Fig. 3. Dimensionless temperature distributions for fluid and solid phases for Models A and B for $\beta = -5$: (a) $Bi = 0.5$ and $k = 0.01$; (b) $Bi = 50$ and $k = 0.01$; (c) $Bi = 0.5$ and $k = 10$; (d) $Bi = 50$ and $k = 10$.

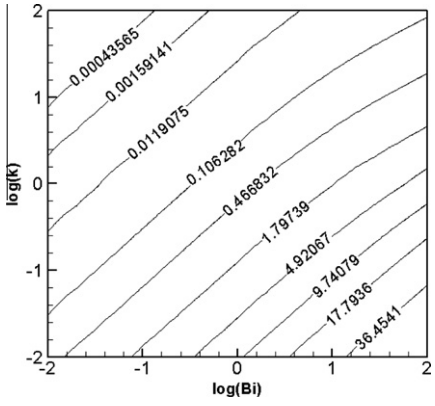

Fig. 4. The variations of β_1 as a function of pertinent parameters Bi and k.

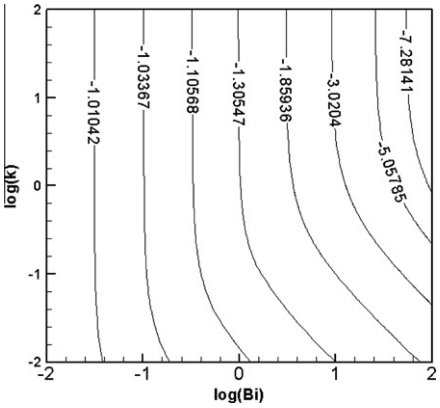

Fig. 5. The variations of β_2 as a function of pertinent parameters Bi and k.

$$q_s = k_{s,eff}\left.\frac{\partial T_s}{\partial y}\right|_{y=H} = q_w\theta_s'(1) \tag{60}$$

Substituting Eq. (54) in Eq. (60), results in

$$q_s = q_w\left\{\frac{1}{1+k} - \left[\frac{1}{(1+k)} + \beta\right]\frac{1}{\lambda}\tanh(\lambda)\right\} \tag{61}$$

Based on Eqs. (59) and (61), the difference between Q and q_s can be expressed as

$$Q - q_s = q_w\beta = S_sH \tag{62}$$

When $\beta > \beta_1$ or $\beta < \beta_2$, and $S_s > 0$, the following inequalities are obtained

$$S_sH > Q > 0 \quad \text{and } S_sH > -q_s > 0 \tag{63}$$

It can be inferred from Eqs. (62) and (63) that, when $\beta > \beta_1$ or $\beta < \beta_2$, and $S_s > 0$, part of the internal heat generation in the solid phase will transfer to fluid phase through the thermal conduction at the wall, instead of through internal heat transfer exchange between the fluid and solid. This paves the way for the occurrence of the temperature gradient bifurcation at the wall. When $\beta = 0$, which translates into no internal heat generation, based on Eq. (55), the temperature gradient directions for the fluid and solid phases at the wall are kept the same. This explains why this phenomenon was not observed in the works of Lee and Vafai [4] and Marafie and Vafai [5]. In their works, the internal heat generation was not included.

Unlike the Nusselt number for the one equation model (based on Eq. (33)), which is just the function of k, the variations of Nusselt number for two-equation model is a function of pertinent

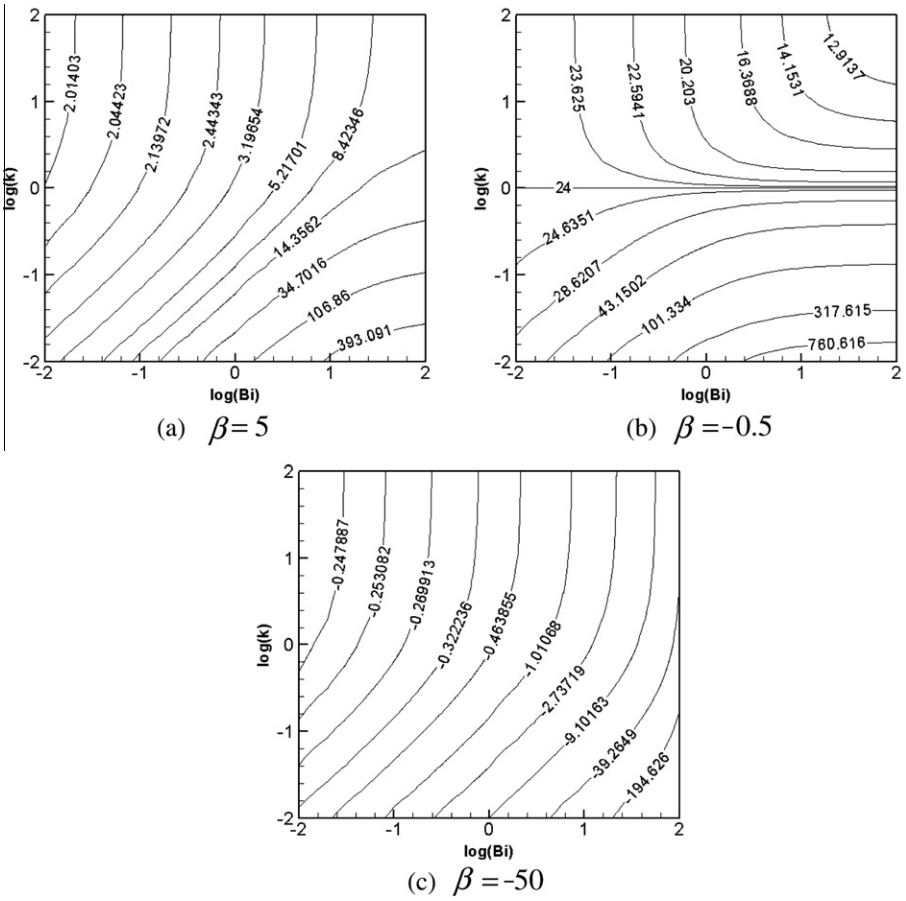

Fig. 6. Nusselt number variations as a function of pertinent parameters β, Bi and k, (a) $\beta = 5$; (b) $\beta = -0.5$; (c) $\beta = -50$.

parameters β, Bi and k as shown in Fig. 6, which is based on Eq. (27). This figure reveals the asymptotic characteristics of the Nusselt number, which can be analyzed using the following relationship [4].

$$\frac{1}{\lambda}\tanh(\lambda) \approx \begin{cases} 1-\lambda^2/3 & \text{as } \lambda \to 0 \\ 0 & \text{as } \lambda \to \infty \end{cases} \tag{64}$$

Based on Eqs. (27) and (64), when $\lambda \to 0$, the asymptotic behavior of the Nusselt number, for Model A, is obtained as

$$Nu \approx \frac{12}{1+\beta} \tag{65}$$

Based on the definition of λ, given in Eq. (21), the condition, $\lambda \to 0$, occurs when

$$Bi \ll \frac{k}{1+k} \tag{66}$$

On the other hand, when $\lambda \to \infty$, the asymptotic behavior of the Nusselt number for Model A is obtained as

$$Nu \approx \frac{4(1+k)}{k}\left[\frac{1}{3}+\left(\frac{1}{1+k}+\beta\right)\frac{1}{Bi}\right]^{-1} \tag{67}$$

Furthermore, when $Bi \to \infty$ and $|\beta| \ll Bi$, the Nusselt number approaches $\frac{12(1+k)}{k}$, i.e.,

$$Nu \approx \frac{12(1+k)}{k} \tag{68}$$

This is the same as the Nusselt number for one equation model. This is because the temperature difference between the fluid and solid phases disappears as $Bi \to \infty$.

It could be seen in Fig. 6 that the Nusselt number for Model A could be either positive or negative for different ranges of β, Bi and k. Based on Eq. (27), if β satisfies the following condition, the Nusselt number, Nu, will be a positive number.

$$\beta > \beta_3 \tag{69}$$

$$\text{where, } \beta_3 = -\frac{Bi}{3\left[1-\frac{1}{\lambda}\tanh(\lambda)\right]} - \frac{1}{1+k} \tag{70}$$

When $\beta \to \beta_3$, the non-dimensionalized bulk mean temperature of the fluid, $\theta_{f,b}$ approaches zero, and the Nusselt number approaches infinity. The variations of β_3 as a function of pertinent parameters Bi and k for Model A, is shown in the Fig. 7. This figure

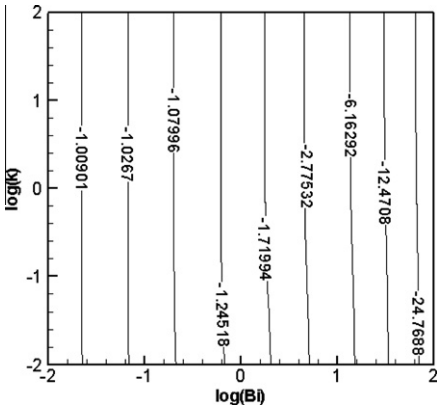

Fig. 7. The variations of β_3 as a function of pertinent parameters Bi and k.

reveals that the thermal conductivity ratio, k, has a substantially smaller influence on β_3 as compared to the Biot number. Comparing Eqs. (57) and (70), one can conclude that

$$\beta_3 \leqslant \beta_2 \tag{71}$$

$$\text{However, when } \lambda \to 0, \beta_2 \approx \beta_3 \to -1 \tag{72}$$

A comparison between the Nusselt number for the LTE Model And that for the LTNE model for the boundary conditions represented by Model A are shown in Fig. 8, in which the error in the Nusselt number based on using the LTE model is evaluated through the analytical solutions given in Eqs. (27) and (33).

$$E = \frac{Nu_1 - Nu}{Nu} = 3\left(\frac{1}{1+k} + \beta\right)\frac{1}{Bi}\left[1 - \frac{1}{\lambda}\tanh(\lambda)\right] \tag{73}$$

For most of the values of the pertinent parameters β, Bi and k, for Model A, the error in using the one equation model is quite large as can be seen in Fig. 8. This difference becomes smaller as the Biot number increases. It should be noted that, for $\beta = -0.5$, the error in using the one equation model becomes zero when $k = 1$, as shown in Fig. 8(b). Based on Eq. (22), when $\beta = -1/(1+k)$, the temperature difference between the fluid and solid phases will disappear, and the Nusselt number for the two-equation model will collapse to that for the one equation model. This criterion is then expressed by:

$$\beta = -\frac{1}{1+k} \tag{74}$$

This is also the reason why the Nusselt number is independent of the Biot number for $k = 1$ in Fig. 6(b). The dimensionless temperature distributions for the fluid and solid phases for Model B for different pertinent parameters β, Bi and k are also shown in the Figs. 2 and 3. When Bi increases, the temperature difference between the two phases becomes smaller. Compared with the results for Model A, the temperature distributions for Model B are quite different. It is found that the temperature gradient for the fluid and solid phases for Model B are always in the same direction at the wall ($\eta = 1$) in Figs. 2 and 3, which is consistent with the boundary condition Eqs. (34) and (35).

For the constant temperature boundary condition, the dimensionless temperature distributions for the solid and the fluid are shown in Fig. 9 for $Bi = 0.5, k = 0.01, \theta_{in} = -16.64, \frac{S_f}{S_s} = \frac{1}{5}$ and $Re = 500$ at $\xi = 2$, $\xi = 5$ and $\xi = 40$. It is found that for this case the phenomenon of temperature gradient bifurcation for the fluid and solid phases at the wall occurs only over a given axial region. For example, for the cited case it occurs at $\xi = 5$, but not at $\xi = 2$ and $\xi = 40$. Another interesting aspect is that after a certain axial length the temperature distribution results from the constant temperature case match the analytical results obtained for the constant heat flux case [Model A]. This situation can be seen in Fig. 9(c).

Fig. 10 shows the heat flux distributions for solid and the fluid at the wall, q_s and q_f, and the corresponding total heat flux distribution, q_w for the constant temperature boundary condition for $Bi = 0.5, k = 0.01, \theta_{in} = -16.64, \frac{S_f}{S_s} = \frac{1}{5}$ and $Re = 500$. It is found that, when $4.24 < \xi < 5.53$, $q_s < 0$ and $q_f > 0$, i.e. the phenomenon of temperature gradient bifurcation for the fluid and solid phases at the wall will occur. When $\xi > 20$, the total heat flux becomes invariant with the axial length, ξ, and $q_w = -(S_s + S_f)H$. This is because when ξ is large enough, all the internal heat generation will be transferred out of the channel through the wall, and the temperatures for solid and fluid phases will remain unchanged. Since the total heat flux does not change when ξ is large enough, we should be able to

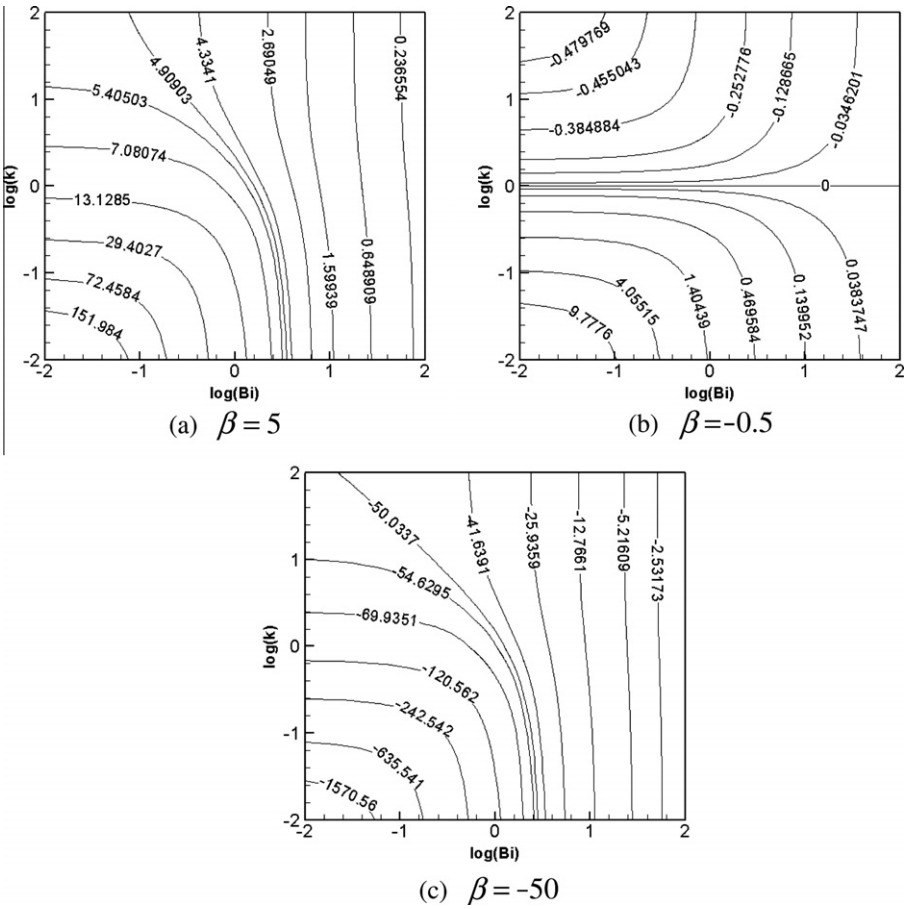

Fig. 8. Nusselt number based error maps when using the LTE model instead of the LTNE model for: (a) $\beta = 5$; (b) $\beta = -0.5$; (c) $\beta = -50$.

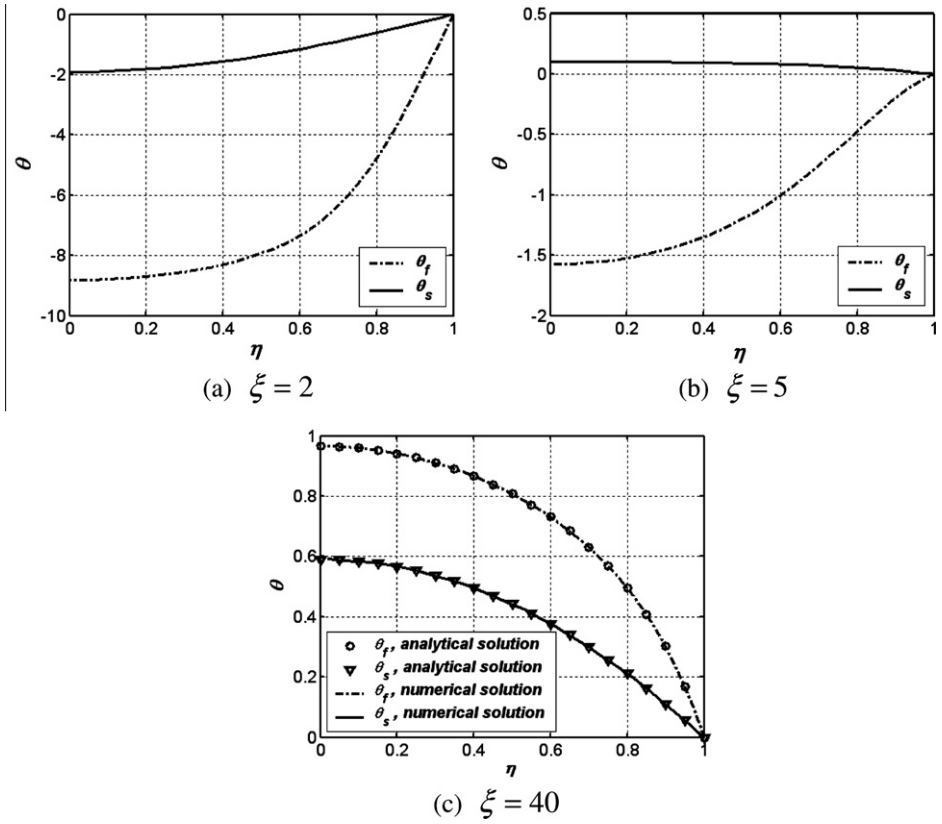

Fig. 9. Dimensionless temperature distributions for the solid and the fluid for constant temperature boundary condition for $Bi = 0.5, k = 0.01, \theta_{in} = -16.64, \frac{S_f}{S_s} = \frac{1}{5}$ and $Re = 500$ at: (a) $\xi = 2$, (b) $\xi = 5$, (c) $\xi = 40$.

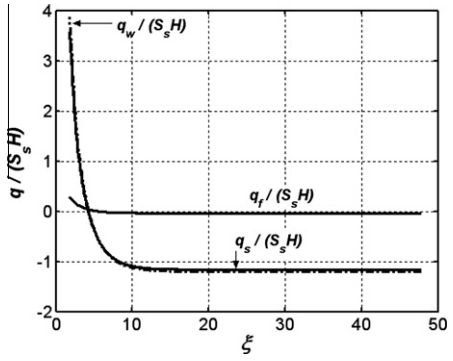

Fig. 10. Heat flux distributions for the solid and the fluid at the wall, q_s and q_f, and the corresponding total heat flux distribution, q_w for the constant temperature boundary condition for $Bi = 0.5, k = 0.01, \theta_{in} = -16.64, \frac{S_f}{S_s} = \frac{1}{5}$ and $Re = 500$.

use our analytical solution for Model A for the constant heat flux boundary condition for this case. Such a comparison was shown earlier in Fig. 9(c). As was mentioned earlier, there is an excellent agreement between the constant temperature solution for larger values of ξ and the analytical solution for the constant heat flux case. It should be noted after the total heat flux becomes invariant, the corresponding β can be presented as $\beta_1 > \beta = -\frac{S_s}{S_s+S_f} > \beta_2$ for $S_s > 0$ and $S_f > 0$. Therefore, based on Eq. (55), the phenomenon of temperature gradient bifurcation will not occur for larger values of ξ.

4. Conclusions

The phenomenon of temperature gradient bifurcation in a porous medium is analyzed in this work. To this end, convective heat transfer within a channel filled with a porous medium subject to a constant wall heat flux boundary condition, with internal heat generation in both the fluid and solid phases, is investigated analytically. A local thermal non-equilibrium (LTNE) model is used to represent the energy transport. Exact solutions are derived for both the fluid and solid temperature distributions for two different primary approaches (Models A and B) for the constant wall heat flux boundary condition. It is shown that the dimensionless temperature distributions for the two phases are independent of the internal heat generation of the fluid phase for both Models A and B. As expected, the temperature difference between the fluid and the solid phases is found to become smaller as the Biot number increases. When Model A is used for the constant wall heat flux boundary condition, the Nusselt number is obtained as a function of the pertinent parameters β, Biot number, Bi and thermal conductivity ratio, k. The internal heat generation in the solid phase is found to have a significant impact on the heat transfer characteristics, represented by the parameter β. It is found that:

(a) When $\beta > \beta_1$ or $\beta < \beta_2$, the phenomenon of temperature gradient bifurcation for the fluid and solid phases at the wall will occur.
(b) When $\beta \to \beta_3$, the Nusselt number will approach infinity.
(c) When $\beta = -1/(1+k)$, the fluid and solid phase temperatures become equal.

The validity of the one equation model is assessed by presenting an error map based on the obtained analytical Nusselt number expressions. It is shown that good agreement between the two models is obtained when $Bi \to \infty$ or $\beta \to -1/(1+k)$.

When Model B is used for the constant wall heat flux boundary condition, the derived temperature distributions are different from those obtained for Model A. The phenomenon of opposite temper-

ature gradient directions for the fluid and solid phases at the wall will not occur when Model B is used. It was shown that the temperature gradient bifurcation can also occur for the constant temperature boundary condition over a given axial length. It was shown that when the axial length is large enough, the temperature gradient bifurcation phenomenon does not occur, and the analytical solution for Model A for the constant heat flux boundary condition can be used for the constant temperature boundary case.

References

[1] M.R.I. Ramadan, A.A. E1-Sebaii, S. Aboul-Enein, E. E1-Bialy, Thermal performance of a packed bed double-pass solar air heater, Energy 32 (2007) 1524–1535.

[2] A. Amiri, K. Vafai, Analysis of dispersion effects and non-thermal equilibrium non-Darcian, variable porosity incompressible flow through porous medium, Int. J. Heat Mass Transfer 37 (1994) 939–954.

[3] A. Amiri, K. Vafai, T.M. Kuzay, Effect of boundary conditions on non-Darcian heat transfer through porous media and experimental comparisons, Numer. Heat Transfer J. A 27 (1995) 651–664.

[4] D.Y. Lee, K. Vafai, Analytical characterization and conceptual assessment of solid and fluid temperature differentials in porous media, Int. J. Heat Mass Transfer 42 (1999) 423–435.

[5] A. Marafie, K. Vafai, Analysis of Non-Darcian effects on temperature differentials in porous media, Int. J. Heat Mass Transfer 44 (2001) 4401–4411.

[6] B. Alazmi, K. Vafai, Constant wall heat flux boundary conditions in porous media under local thermal non-equilibrium conditions, Int. J. Heat Mass Transfer 45 (2002) 3071–3087.